



Bladder overactivity and afferent hyperexcitability induced by prostate-to-bladder cross-sensitization in rats with prostatic inflammation

Yasuhito Funahashi^{1,3}, Ryosuke Takahashi^{1,4}, Shinsuke Mizoguchi¹, Takahisa Suzuki¹, Eiichiro Takaoka¹, Jianshu Ni¹, Zhou Wang¹, Donald B. DeFranco², William C. de Groat², Pradeep Tyagi¹  and Naoki Yoshimura^{1,2} 

¹Departments of Urology, University of Pittsburgh School of Medicine, Pittsburgh, PA 15213, USA

²Pharmacology and Chemical Biology, University of Pittsburgh School of Medicine, Pittsburgh, PA 15213, USA

³Department of Urology, Nagoya University Graduate School of Medicine, Aichi 466–8550, Japan

⁴Department of Urology, Kyusyu University Graduate School of Medicine, Fukuoka 812–8582, Japan

Edited by: Kim Barrett & Weifang Rong

Key points

- There is clinical evidence showing that prostatic inflammation contributes to overactive bladder symptoms in male patients; however, little is known about the underlying mechanisms
- In this study, we investigated the mechanism that prostatic inflammation causes detrusor overactivity by using a rat model of chemically induced prostatic inflammation.
- We observed a significant number of dorsal root ganglion neurons with dichotomized afferents innervating both prostate and bladder.
- We also found that prostatic inflammation induces bladder overactivity and urothelial NGF overexpression in the bladder, both dependent on activation of the pelvic nerve, as well as changes in ion channel expression and hyperexcitability of bladder afferent neurons.
- These results indicate that the prostate-to-bladder cross-sensitization through primary afferent pathways in the pelvic nerve, which contain dichotomized afferents, could be an important mechanism contributing to bladder overactivity and afferent hyperexcitability induced by prostatic inflammation.

Abstract Prostatic inflammation is reportedly an important factor inducing lower urinary tract symptoms (LUTS) including urinary frequency, urgency and incontinence in patients with benign prostatic hyperplasia (BPH). However, the underlying mechanisms inducing bladder dysfunction after prostatic inflammation are not well clarified. We therefore investigated the effects of prostatic inflammation on bladder activity and afferent function using a rat model of non-bacterial prostatic inflammation. We demonstrated that bladder overactivity, evident as decreased voided volume and shorter intercontraction intervals in cystometry, was observed

Yasuhito Funahashi and Ryosuke Takahashi performed the experiments in the laboratory of Dr Yoshimura at the University of Pittsburgh as Research Associates. The laboratory focuses primarily on functional and physiological changes of the lower urinary tract and has published extensively on how pathophysiological conditions including spinal cord and peripheral nerve injuries, inflammation and diabetes mellitus trigger hyperexcitability of the visceral neuronal pathways innervating the lower urinary tract and how neurotrophic factors control neuronal activities.



Y. Funahashi and R. Takahashi contributed equally as co-first authors to this study.

in rats with prostatic inflammation *versus* controls. Tissue inflammation, evident as increased myeloperoxidase activity, and IL-1 α , IL-1 β , and IL-6 levels inside the prostate, but not in the bladder, following intraprostatic formalin injection induced an increase in NGF expression in the bladder urothelium, which depended on activation of the pelvic nerve. A significant proportion (18–19%) of dorsal root ganglion neurons were double labelled by dye tracers injected into either bladder or prostate. In rats with prostatic inflammation, TRPV1, TRPA1 and P2X2 increased, and Kv1.4, a potassium channel α -subunit that can form A-type potassium (K_A) channels, decreased at mRNA levels in bladder afferent and double-labelled neurons *vs.* non-labelled neurons, and slow K_A current density decreased in association with hyperexcitability of these neurons. Collectively, non-bacterial inflammation localized in the prostate induces bladder overactivity and enhances bladder afferent function. Thus, prostate-to-bladder afferent cross-sensitization through primary afferents in the pelvic nerve, which contain dichotomized afferents, could underlie storage LUTS in symptomatic BPH with prostatic inflammation.

(Resubmitted 16 November 2018; accepted after revision 9 January 2019; first published online 22 January 2019)

Corresponding author Naoki Yoshimura: Department of Urology, University of Pittsburgh School of Medicine, 3471 Fifth Avenue, Pittsburgh, PA 15213, USA. Email: nyos@pitt.edu

Introduction

There is increasing evidence showing that inflammation of one pelvic organ such as the urinary bladder or the colon may lead to neurogenic inflammation and/or referred pain in another by means of shared neural pathways connecting different pelvic organs (Malykhina, 2007; Brumovsky & Gebhart, 2010). The cross-sensitization between two organs could occur at three different afferent levels: an antidromic axon reflex via dichotomizing afferent neurons in dorsal root ganglia (DRG), viscerosomatic convergence in the spinal cord (afferent-afferent interactions via the spinal cord) or interactions of neural pathways in the brain. Previous studies have demonstrated that a significant number of dichotomized DRG neurons innervate both bladder and prostate (Chen *et al.* 2010; Lee *et al.* 2016a).

Lower urinary tract symptoms (LUTS) are commonly seen in males with benign prostatic hyperplasia (BPH), and storage LUTS such as urinary frequency and urgency overlap with those of overactive bladder. BPH-induced bladder outlet obstruction (BOO) has been proposed as a mechanism inducing enhanced bladder afferent activity and storage LUTS due to various factors including decreased release of nitric oxide (Kim *et al.* 2011), increased release of prostaglandin E2 from the urothelium (Beppu *et al.* 2011), decreased potassium channel activity (Aydin *et al.* 2012), or ischaemia and oxidative stress to the detrusor (Lin *et al.* 2008). However, the size of prostate and LUTS severity do not always correlate and patients sometimes suffer LUTS even in the absence of prostate enlargement, which suggests that multiple factors contribute to the pathogenesis of LUTS (Funahashi *et al.* 2011; Chung *et al.* 2012). In this regard, intra-prostatic inflammation has been proposed to be involved in the development of LUTS. There are increasing clinical reports

of association between the LUTS scores and the degree of prostatic inflammation in BPH specimens (Nickel *et al.* 2008; Robert *et al.* 2009; Fibbi *et al.* 2010; Liao *et al.* 2011; Chung *et al.* 2012), and it is possible that afferent cross-sensitization between the prostate and bladder due to prostatic inflammation could be another mechanism inducing storage LUTS in BPH patients.

Rodent models of non-bacterial or bacterial prostatic inflammation show bladder overactivity evident by frequent voiding (Chen *et al.* 2010; Lee *et al.* 2015; Schwartz *et al.* 2016; Mizoguchi *et al.* 2017). However, detailed functional and molecular mechanisms underlying bladder dysfunction following prostatic inflammation remain to be elucidated. In this study, we therefore examined changes in bladder activity and molecular and functional properties of DRG neurons innervating the prostate and/or bladder in a rat model of chemically induced prostatic inflammation to investigate the inflammation-related mechanisms underlying male LUTS due to BPH with prostatic inflammation.

Methods

Ethical approval

All animal experiments were conducted in accordance with the ARRIVE and NIH guidelines and approved by the Institutional Animal Care and Use Committees (IACUC) (Protocol approval no. 15086776). Efforts were made to minimize the suffering of the animals and the number of animals needed to obtain reliable results.

Animal surgery

Male Sprague-Dawley rats weighing 150–200 gm ($n = 110$ rats in total) were anaesthetized with isoflurane and, in

a supine position, the prostate and bladder were exposed with a lower abdominal incision. To produce a chemically induced prostatic inflammation model, formalin (5% in saline) or saline (vehicle control) was injected into each ventral lobe of the prostate (50 μ l per lobe) as previously reported (Funahashi *et al.* 2014). In a separate group of rats used for analyses of the distribution of fluorescent dye-labelled DRG cells, laser-capture microdissection (LCM), and whole-cell patch clamp recordings, 0.2% 1,1'-dioctadecyl-3,3,3',3'-tetramethylindocarbocyanine perchlorate (DiI) in 2% dimethyl sulfoxide in 5% formalin or saline was injected into each ventral lobe of the prostate (50 μ l per lobe), and 1% Fast Blue in saline (20 μ l) was injected in the posterior wall of the bladder (4 sites, 5 μ l per site). To decrease dye leakage, the needle tip was tunnelled 2–3 mm subserosally and the needle was held in place for 10 s after each injection. In addition, each puncture site was swabbed with fresh cotton-tipped applicators to absorb any potential tracer leakage. The abdominal incision was closed after injection, and all experiments were performed 1 week later.

Histological analyses

The ventral lobes of prostate and the bladder were excised 1 week after surgery, embedded in OCT Tissue Tek (Sakura Finetek U.S.A, Torrance, CA, USA), frozen in liquid nitrogen, and kept at -80°C until use. Samples were serially sectioned at 8 μ m thickness, and microscopic examination was conducted in tissue sections stained with Haematoxylin and Eosin.

Measurement of inflammatory markers

The prostate and bladder tissues of formalin- and saline-injected rats ($n = 6$ per groups) were homogenized using RIPA lysis buffer. Homogenate was centrifuged at 10,000 g for 10 min and the supernatants were stored at -80°C until assayed. IL-1 α , IL-1 β , and IL-6 levels were determined by the Luminex 200 (Bio-Rad, Hercules, CA, USA) using a MILLIPLEX MAP Rat Cytokine/Chemokine Panel (Millipore, Billerica, MA, USA). Myeloperoxidase (MPO) concentration, which is indicative of neutrophil activity, was measured using specific enzyme-linked immunosorbent assay (ELISA) kits (Hycult Biotech, Plymouth Meeting, PA, USA). Protein concentration was determined using a Bio-Rad kit with bovine serum albumin as the standard. The cytokine and MPO concentrations were standardized to tissue protein levels and expressed in pico- or nanograms per milligram total protein, respectively.

Voiding behavioural studies

Formalin- or saline-injected rats ($n = 6$ per groups) were placed in a metabolic cage before and 1-week after

the treatment. Voided urine was collected continuously using a cup placed beneath the metabolic cage and fitted onto a Fort 100 force displacement transducer connected to a Transbridge TBM4M amplifier (World Precision Instruments, Sarasota, FL, USA) to measure voided volume. Data were collected using a data acquisition system equipped with a Power Lab analogue-to-digital converter (AD Instruments, Milford, MA, USA). The overnight monitoring period started at 19.00 h and ended at 07.00 h. All rats had free access to water and food during the recording period in the cage. The variables of micturition obtained included micturition frequency, total urine output and single voided volume.

Conscious cystometry

One week after intraprostatic injection of formalin ($n = 7$) or saline ($n = 6$), rats were anaesthetized with iso-flurane. Following a lower midline abdominal incision, the bladder was exposed and catheterized with PE-50 tubing (Clay Adams Division of Becton Dickinson, Parsippany, NJ, USA) inserted through the bladder dome. After recovery from anaesthesia, conscious rats were placed in a restraining cage. After 2 h of acclimation, saline was infused into the bladder at 0.04 ml min $^{-1}$, and rats voided spontaneously through the urethra. At least four reproducible micturition cycles were recorded after an initial stabilization period (60 min). A software package (Chart5 software) (ADInstrument, Milford, MA, USA) was used for data collection and analysis. Baseline pressure, pressure threshold for voiding, peak voiding pressure and intercontraction interval were evaluated.

In addition, bladder activity was evaluated in a separate group of rats with transection of the right pelvic nerve to examine whether bladder functional changes after prostatic inflammation is nerve-mediated and dependent on pelvic nerve activation. In these animals, formalin was injected into the ipsilateral (right) or contralateral (left) side of the ventral prostate lobe following pelvic nerve transection ($n = 7$ and 8, respectively). Then, single cystometry was performed under an awake condition 1 week after formalin injection and the data were compared with pelvic nerve-transected rats without formalin injection ($n = 7$).

Retrograde fluorescence labelling of DRG neurons

At 1 week after dye injection into the prostate or bladder, Th13 to S2 DRG of formalin- and vehicle-injected rats (6 DRG from 3 rats per groups) were excised, embedded in OCT Tissue Tek, frozen in liquid nitrogen, and kept at -80°C until use. Samples were serially sectioned at 8 μ m thickness, and every third section was mounted onto slides to avoid repeat counting of the cells. The slides were observed using a fluorescence microscope with

appropriate filters, and the numbers of Fast Blue-labelled, DiI-labelled, or double-labelled cells were counted and expressed as the average of positive cells per section in each ganglion.

Dissociation of DRG neurons and whole-cell patch-clamp recording

In a separate group of rats injected with dye tracers, freshly dissociated neurons from L6-S1 DRG were prepared from formalin- or saline-injected rats ($n = 18$ each), as described previously (Yoshimura & de Groat, 1997). L6 DRG on both sides and S1 DRG on one side were removed, minced and incubated for 25 min at 35°C in 5 ml DMEM (Sigma, St Louis, MO, USA) containing 0.5 mg/ml trypsin (Sigma), 1 mg/ml collagenase (Type I, Sigma). Trypsin inhibitor (Sigma) was then added to neutralize the enzyme activity. Individual DRG cell bodies were isolated by trituration and plated on poly-L-lysine-coated 35 mm culture dishes.

Whole-cell patch-clamp recordings were performed at room temperature (20–22°C) on Fast Blue- and/or DiI-positive neurons within 10 h of dissociation. The internal solution contained (in mM): 140 KCl, 1 CaCl₂, 2 MgCl₂, 11 EGTA, 10 HEPES, 2 Mg-ATP adjusted to pH 7.4 with KOH. Patch electrodes had resistances of 2–4 MΩ when filled with the internal solution. Neurons were superfused initially at a flow rate of 2.0 ml min⁻¹ with an external solution containing (in mM): 150 NaCl, 5 KCl, 2.5 CaCl₂, 1 MgCl₂, 10 HEPES, and 10 D-glucose, adjusted to pH 7.4 with NaOH, to evaluate the action potential properties under the current clamp condition. Thereafter, to isolate K⁺ currents under the voltage-clamp condition, as previously described (Yoshimura *et al.* 2006), neurons were superfused with an external solution containing 110 mM choline-Cl, 5 mM KOH, 0.03 mM CaCl₂, 3.4 mM Mg(OH)₂, 10 mM HEPES and 10 mM D-glucose, adjusted to pH 7.4 with Trizma hydrochloride (340 mOsm), which suppresses Na⁺ and Ca²⁺ currents (Yoshimura & de Groat, 1999).

After evaluation of action potential characteristics or isolation of K⁺ currents, capsaicin sensitivity was evaluated by direct application of capsaicin (500 nM) to the neurons in a voltage-clamp mode with a holding potential (HP) at -60 mV. Inward shift of holding currents was observed in capsaicin-sensitive neurons. The stock solution of capsaicin (Sigma-Aldrich) at 5 mM containing 10% ethanol and 10% Tween 80 was prepared in the external solution described above for action potentials evaluation, and then diluted to the final concentration in the same external solution before experiments. All recordings were made with an Axopatch 700B patch-clamp amplifier and controlled by Clampex software (Axon Instruments, Sunnyvale, CA, USA). Data were then analysed by pCLAMP software (Axon Instruments). Cell

membrane capacitances were obtained by reading the value for whole-cell input capacitance neutralization directly from the amplifier. Data are presented from neurons that exhibited resting membrane potentials greater than -40 mV and action potentials that overshoot 0 mV.

LCM and RNA isolation and real-time PCR analysis

S1 DRG from formalin- ($n = 11$) or vehicle-injected rats ($n = 10$) with dye injections were embedded in Tissue Tek OCT. Sections were cut at 8 μm thickness and mounted on PEN membrane slides (Leica Microsystems, Wetzlar, Germany). LCM was performed using a Leica LMD6000 microscope (Leica Microsystems). Twenty cells that were labelled with either Fast Blue, DiI, or both, and 20 unlabelled cells from S1 DRG sections in each rat were excised and captured in 0.5 ml Eppendorf tube caps, separately. Captured specimens were lysed and RNA isolation, DNase digestion, reverse transcription and real-time PCR were performed using the Cells Direct TM One-Step qRT-PCR Kit (Invitrogen, Carlsbad, CA, USA) for transient receptor potential (TRPV) 1, TRPA1, Kv1.4, P2X2 and P2X3 (Table 1). Gene-specific primers and Taqman probes were designed with Primer 3 Software (Primer 3, Totowa, NJ, USA). All probes spanned the exon-exon junction and contained FAM fluorophore and TAMRA quencher. The primer and probe combination were optimized within suitable ranges for efficiency and correlation coefficient using standard curve dilutions and data output on the ABI Step-One Plus thermocycler (Applied Biosystems). Amplification of cDNA was performed under the following conditions: one cycle of 50°C for 15 min, then 95°C for 2 min, followed by 40 cycles of 15 s at 95°C, then 45 s at 60°C. The reactions were analysed in triplicate and normalized to GAPDH. Real-time PCR data were analysed by DCp (crossing point) method as $R = 2^{-(Cp \text{ sample} - Cp \text{ control})}$ to generate the relative expression ratio of each target gene relative to GAPDH. The mean value for each group of labelled neurons was then divided by the mean value for the non-labelled neurons to evaluate the ratio changes in each molecule after prostatic inflammation.

To determine the specificity of the primer/probe, we performed electrophoresis to check that the optical band was amplified without non-specific bands. We also determined specificity to cDNA to identify that our primer/probe set did not amplify genomic DNA by electrophoresis.

Immunohistochemistry for nerve growth factor (NGF)

The bladder sections (8 μm) obtained from vehicle- and formalin-injected rats ($n = 3$ each) were directly mounted

Table 1. Sequences of primers and probes

	5' primer	3' primer	Taqman probe	Efficacy (%)
TRPV1	CCGGAGAGATCTTGTCTGTG	ACCAGCATGAACAGCGACT	TATTCCTGCAGAGGCGACCATCC	95.7
TRPA1	ATCAGGAGACCCTGCTTCAC	GTTGATGTCTGCTCCACTG	TGATCATCATGACCTGGCAGACTACC	101.3
Kv 1.4	TGACCTACTGCCACAGGATG	GGTTTCGAAGCGTAGACCAG	CAGTGACTGTTGTGAACGCGTGGT	104.4
P2X2	GCATCATCACCAGGATCGAG	GTCTTGGAGTCCCATGGTA	TCAGACGACGACTGTATTGCCGGA	102.2
P2X3	GGCTGGATGGAGTTTCTGAG	TTCAGGAGTGTCCGGTACTC	CCCTGGCTACAACCTCAGGTTTGCC	104.4
GAPDH	AGACAGCCGCATCTTCTGT	GATACGGCCAAATCCGTTT	GCAGTGCCAGCCTCGTCTCA	104.0

on coated slides and fixed with 4% paraformaldehyde for 10 min, rinsed with phosphate-buffered saline (PBS), transferred to 3% hydrogen peroxide for 10 min to block peroxidase activity, and rinsed with distilled water and PBS. Next, the sections were blocked with 10% normal goat serum (Invitrogen, Grand Island, NY, USA) for 30 min. Without rinsing, the tissues were reacted with anti-NGF antibody (1:1000) (Abcam, Cambridge, MA, USA) for 1 h at room temperature, and washed with PBS. The tissues were then incubated for 30 min with HRP-labelled polymer anti-rabbit antibody (Dako, Carpinteria, CA, USA) at room temperature and rinsed with PBS. For streptavidin–horseradish peroxidase detection, the tissues were stained with avidin–biotin complex reagent (Dako) for 10 min at room temperature. Haematoxylin staining was used for counterstaining.

Western blotting for NGF

For the quantitative analysis of NGF expression changes, the bladder tissue homogenate from formalin- or saline-injected rats ($n = 6$ per group) was dissolved in $2 \times$ sample buffer (Bio Rad, Hercules, CA, USA) with 5% β -mercaptoethanol and denatured at 95°C for 5 min. Bladder homogenate samples were also obtained from the bladder mucosa of right pelvic nerve-transected rats with or without intraprostatic formalin injection ($n = 7$ – 8 per group). Equivalent amounts of protein (30 μ g) were separated by SDS-PAGE electrophoresis using 10% TBE Precast Gels (Bio Rad) and transferred onto a PVDF membrane (Millipore). Membranes were blocked with 0.5% ECL Blocking Agent (GE Healthcare, Piscataway, NJ, USA) in PBS with 0.1% Tween-20 at 4°C overnight and incubated for 1 h at room temperature with the anti-NGF antibody (1:250). The blots were then incubated for a further 1 h at room temperature with an HRP-conjugated secondary antibody (1:1000; Cell Signalling Technology, Danvers, MA, USA). Specific protein signals were visualized using the ECL Plus Western Blotting Detection System (GE Healthcare). The intensity of the protein bands was semiquantitatively analysed by Image J software.

Statistics

Data are presented as mean values \pm standard error of the mean. Student's unpaired t test was used to test for statistical differences between two groups. Holm–Sidak's multiple comparisons test was used for statistical analyses among groups of more than two. All tests were two-sided, and P values < 0.05 were considered statistically significant. All statistical analyses were performed using SPSS software.

Results

Histopathology

Macroscopically, the formalin-injected prostate showed a slightly atrophic appearance compared to vehicle-injected prostate, and there was no difference in the ventral lobe prostate weight between vehicle- and formalin-injected groups (372 ± 12 vs. 326 ± 22 mg, $n = 5$ each). Compared to the prostate of vehicle-treated controls, microscopic examination of the formalin-injected prostate demonstrated mild inflammation in most areas of the ventral lobe prostate and severe inflammation in some areas, with infiltrating leukocytes, expansion of stromal area and atrophic epithelium (Fig. 1A–C). The bladder wall showed no evidence of inflammation in either group (Fig. 1D and E).

Measurement of inflammatory markers

Levels of IL-1 α , IL-1 β and IL-6 in the formalin-injected prostate were significantly increased by 2- to 3-fold compared to vehicle-treated controls (Fig. 2A–C). However, in the bladder there were no significant differences between groups. Similarly, MPO activity of the prostate was increased in formalin-injected rats compared to vehicle-injected rats; whereas there were no significant differences in the bladder (Fig. 2D). Taken together with histological findings, these results indicate that formalin-induced inflammation was restricted to the prostate.

Voiding behavioural studies

There was no significant difference in total urine volume, the number of voids, or single voided volume between the two groups before formalin or vehicle treatment (Table 2A). None of these parameters was altered in vehicle-treated rats at 1 week; however, in formalin-treated rats the number of voids increased and single voided volume decreased significantly compared to pre-treatment values.

Conscious cystometry

Cystometric parameters were measured during repetitive voiding cycles after a 60-min acclimation period. The mean intercontraction interval was 999 ± 57 s in the formalin-injected group *vs.* 1483 ± 26 s in vehicle-injected controls ($P < 0.05$), and the number of non-voiding contractions (NVC) during the storage phase was increased in formalin-injected rats *vs.* vehicle-injected rats (4.25 ± 0.71 *vs.* 0.33 ± 0.25 /voiding cycle) (Fig. 3 and Table 2B). Baseline pressure, pressure threshold for voiding and peak voiding pressure were not different between two groups. In addition, in rats with transection of the right pelvic nerve, bladder overactivity evident as increased NVCs was not induced after formalin injection into the right ventral lobe of prostate, but was still observed after the left lobe injection (Fig. 4).

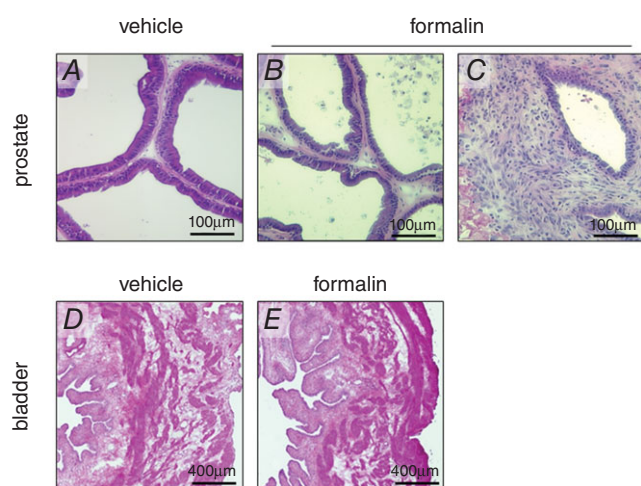


Figure 1. Histological findings of bladder and prostate sections

Haematoxylin and eosin staining showed that intra-prostatic formalin injection caused either a low-grade inflammation (B) or high-grade inflammation (C) in the prostate compared to the vehicle-injected prostate (A). There were no inflammatory changes in the bladder of vehicle (D) or formalin-treated rats (E). Scale bars; 100 μ m (A–C); 400 μ m (D and E).

Distribution of fluorescent-labelled neurons

Fast Blue-labelled bladder afferent and DiI-labelled prostate afferent neurons were identified as blue- and red-coloured cells, respectively, in DRG sections using appropriate filters (Fig. 5). Some neurons were labelled with both Fast Blue and DiI, indicative of dichotomized neurons. Dye-labelled neurons were mainly observed in L1, L6 and S1 DRG, and these distributions were similar between vehicle- and formalin-injected rats, without significant differences in the number of labelled neurons per DRG section between two groups (data not shown). Double-labelled (e.g. DiI- and Fast Blue-positive) afferent neurons innervating both prostate and bladder represented 18.4% of the total number of DiI- and Fast Blue-labelled neurons in thoraco-lumbar DRG and 19.5% in lumbo-sacral DRG.

Electrophysiology

It has been reported that C-fibre bladder afferent hyperexcitability is an important contributing factor to bladder overactivity in various pathophysiological conditions such as bladder outlet obstruction, spinal cord injury and bladder inflammation (de Groat *et al.* 2015). Therefore, this study focused on the changes in electrophysiological properties of the C-fibre population of prostate and/or bladder afferent neurons. Because our previous study demonstrated that the majority (80%) of C-fibre bladder afferent neurons are sensitive to capsaicin, while only a small population (5%) of A δ -fibre bladder neurons are capsaicin sensitive (Yoshimura *et al.* 1998), bladder afferent neurons that exhibited capsaicin (500 nM)-induced inward currents in voltage-clamp recordings at the end of patch-clamp recordings are included in the analyses in the present study.

In preliminary experiments, we found similar changes in firing pattern of action potentials in DiI-labelled prostate afferent neurons and double-labelled prostate/bladder afferent neurons after prostatic inflammation. Therefore, we here described the electrophysiological results obtained from double-labelled afferent neurons. In capsaicin-sensitive, double-labelled afferent neurons innervating both bladder and prostate, the resting membrane potential did not differ between vehicle- and formalin-injected rats (Table 3 and Fig. 6). However, the mean threshold for eliciting action potentials in formalin-injected rats (-28.3 ± 1.4 mV) was significantly lower than that in control rats (-19.5 ± 1.1 mV); and the number of action potentials during 800 ms membrane depolarization in rats with prostatic inflammation (5.1 ± 0.7 spikes) was significantly higher than that in control rats (1.2 ± 0.1 spikes), when the current intensity was set to the value just above the threshold for inducing a single action potential

with a 50-ms depolarization. Furthermore, the mean spike amplitude (46.3 ± 2.6 mV) was significantly higher and the mean spike duration (3.6 ± 0.4 ms) was significantly shorter than the measurements in control rats (36.3 ± 2.2 mV and 6.4 ± 0.9 ms, respectively). These results indicate that capsaicin-sensitive, double-labelled dichotomized afferent neurons become hyperexcitable in rats with prostatic inflammation. In addition, the cell input capacitance of capsaicin-sensitive double-labelled afferent neurons from formalin-injected rats (37.5 ± 3.2 pF) was significantly greater than in neurons from control rats (27.0 ± 1.5 pF), indicating that prostatic inflammation induced somal hypertrophy of these neurons.

In capsaicin-sensitive bladder afferent neurons that were labelled only by Fast Blue, the resting membrane potential was not affected by prostate inflammation; however, the mean threshold for eliciting action potentials in formalin-injected rats (-28.7 ± 1.4 mV) was significantly lower than that in control rats (-21.6 ± 2.4 mV), and the number of action potentials during 800 ms membrane depolarization in formalin-injected rats (3.5 ± 0.4 spikes) was significantly greater than that in control rats (1.5 ± 0.3 spikes).

We previously reported that the reduction of slow K_A currents is involved in increased excitability of capsaicin-sensitive bladder afferent neurons in rat models of cystitis or spinal cord injury (Yoshimura & de Groat, 1999; Hayashi *et al.* 2009; Takahashi *et al.* 2013). Because we found similar changes in firing pattern of action potentials in both prostate/bladder and bladder afferent neurons, we further evaluated the properties of potassium currents in bladder afferent neurons from vehicle- or formalin-injected rats. An estimate of the density of slow K_A currents in these neurons was obtained by measuring the difference in the currents activated by a depolarizing voltage pulse from -120 mV and -40 mV holding potentials (Fig. 7A and B). This method is useful because our previous studies showed that slow K_A currents in capsaicin-sensitive C-fibre bladder afferent neurons were activated by depolarizing voltage steps from hyperpolarized membrane potentials but were almost completely inactivated when the membrane potential was maintained at a depolarized level of more than -40 mV (Yoshimura & de Groat, 1999; Takahashi *et al.* 2013). As shown in Fig. 7C, peak current densities of slow K_A currents evoked by depolarization up to 30 mV, which was calculated from the difference in

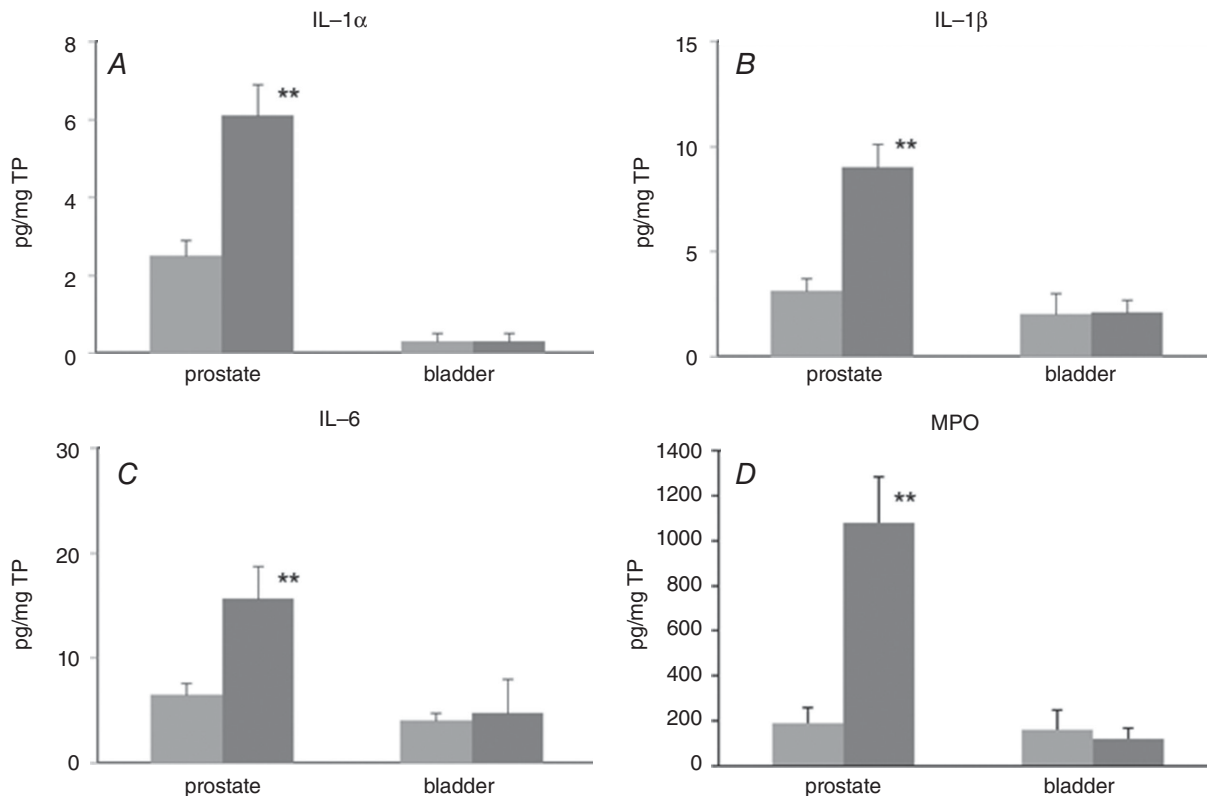


Figure 2. Inflammatory markers

Proinflammatory cytokine levels (A, IL-1 α ; B, IL-1 β ; C, IL-6) and MPO activity were measured in the prostate and bladder using ELISA. Light grey columns, vehicle-treated rats. Dark grey columns, formalin-treated rats. $n = 6$ in each group. Columns with bars represent mean \pm SEM. ** $P < 0.01$ between groups. TP, total protein.

Table 2. Urodynamic evaluation

A. Voiding behaviour	Vehicle (n = 6)		Formalin (n = 6)	
	before	After	before	after
Urine volume (ml)	7.8 ± 1.3	7.5 ± 0.7	9.1 ± 2.2	7.9 ± 1.4
No. of micturition (per day)	18.2 ± 1.8	18.5 ± 1.1	18.7 ± 2.6	25.5 ± 4.3
Single voided volume (ml)	0.42 ± 0.03	0.41 ± 0.03	0.46 ± 0.08	0.33 ± 0.07**
B. Cystometry	Vehicle (n = 6)		Formalin (n = 7)	
Baseline pressure (cmH ₂ O)	3.6 ± 1.5		5.1 ± 1.3	
Threshold pressure (cmH ₂ O)	8.4 ± 1.5		9.0 ± 1.2	
Peak pressure (cmH ₂ O)	39.0 ± 2.6		34.5 ± 2.1	
Intercontraction interval (s)	1483 ± 26		999 ± 57*	
No. of non-voiding contractions per voiding cycle	0.33 ± 0.25		4.25 ± 0.71*	

* $P < 0.05$ between vehicle and formalin groups; ** $P < 0.01$ between the values before and after injection.

K⁺ currents activated from holding potentials of -40 and -120 mV, were significantly smaller ($P < 0.05$) at depolarizing pulses greater than -20 mV in neurons from formalin-injected rats compared to those from vehicle-injected rats. However, the peak current density of sustained K_{DR} currents in capsaicin-sensitive bladder afferent neurons was not different between formalin- and vehicle-injected rats (Fig. 7D). Taken together, these results indicate that capsaicin-sensitive bladder afferent neurons become hyperexcitable at least in part due to the reduction in slow K_A current activity following prostatic inflammation.

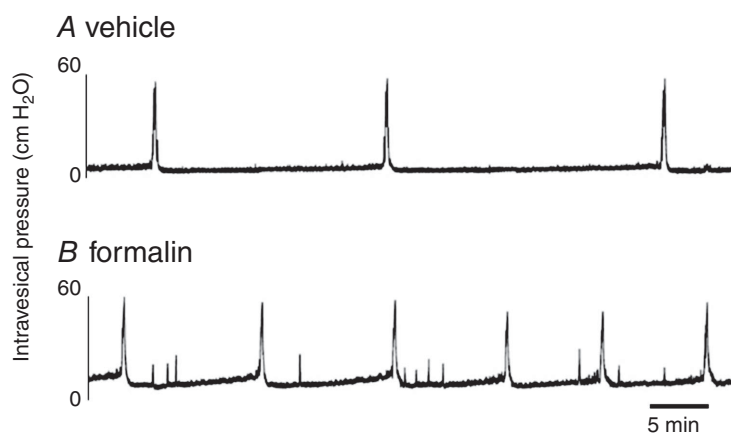
mRNA expression in DRG neurons

We measured mRNA levels of TRPV1, TRPA1, P2X2, P2X3 and the Kv1.4 potassium channel subunit of Fast Blue-, DiI-, double-labelled and non-labelled neurons obtained by LCM from formalin- and vehicle-injected rats. The Kv1.4 α -subunit was chosen because we have previously shown that the decreased expression of this subunit is associated with increased excitability and a

reduction in slow K_A channel activity in bladder afferent neurons after cystitis or spinal cord injury (Hayashi *et al.* 2009; Takahashi *et al.* 2013). In vehicle-injected rats, there were no significant changes in mRNA levels of any of these channels in dye-labelled neurons when compared to non-labelled neurons (Fig. 8). In contrast, TRPV1, TRPA1 and P2X2 were up-regulated, and Kv1.4 was down-regulated significantly in dye-labelled cells vs. non-labelled cells in formalin-injected rats. The P2X3 mRNA level in labelled cells of either group was not altered compared to the level of non-labelled cells.

NGF expression in the bladder

In the bladder of formalin-injected rats, immunohistochemistry showed increased expression of NGF, which was most obvious in the urothelium, but also evident in the submucosal layer (Fig. 9A–D). Western blotting was then performed for quantitative analyses and showed that NGF expression (normalized to β -actin) in the whole bladder was significantly higher in the formalin-injected rats compared to vehicle-injected rats

**Figure 3. Continuous cystometry**

Representative traces of cystometry under an awake condition in vehicle- (A) or formalin-injected rats (B). Cystometric parameter analyses showed that intercontraction intervals were shorter and the number of non-voiding contraction during urine storage in formalin-injected was greater than those in vehicle-injected rats, indicating bladder overactivity after prostatic inflammation.

(2.22 ± 0.37 vs. 1.00 ± 0.23 , $P = 0.019$). In addition, in rats with the right pelvic nerve transection (PNT), formalin injection into the left ventral lobe of prostate induced NGF upregulation in the bladder mucosa compared to PNT alone rats (1.59 ± 0.13 vs. 1.00 ± 0.04 , $P = 0.009$), which was prevented when formalin was injected into the right ventral lobe of prostate (0.98 ± 0.09 vs. 1.00 ± 0.04 , $P = 0.865$).

Discussion

Our detailed molecular, cellular and electrophysiological analysis following intra-prostatic injection of formalin in rats revealed a number of potential mechanisms that could contribute to various functional outcomes of the resulting prostatic inflammation. For example, formalin-induced non-bacterial inflammation after intra-prostatic injection is limited to the prostate, without an extension to the bladder. Furthermore, prostatic inflammation induces bladder overactivity as evidenced by reductions in volume per void and intercontraction intervals. In addition, because the prostatic weight was not altered after formalin injection, prostate enlargement was not likely to be involved in bladder functional changes in this model. We also identified a considerable number of DRG neurons with dichotomized afferent nerves that innervate both prostate and bladder that are distinguished by a number of responses to inflammation. The proportion of DRG neurons with dichotomized afferents labelled by dye

tracers from the prostate and the bladder (18–19%) in this study was comparable to those previously reported in rats (14%) (Chen *et al.* 2010) and mice (17%) (Schwartz *et al.* 2016). Specifically, prostatic inflammation induces upregulation of TRPV1, TRPA1 and P2X2 expression and downregulation of Kv1.4 not only in prostate afferent neurons, but also in dichotomized afferent neurons innervating both organs, as well as bladder afferent neurons that do not innervate the prostate. Prostatic inflammation induces functional changes such as hyperexcitability of capsaicin-sensitive C-fibre afferent neurons in association with downregulation of slow K_A current density. Finally, NGF expression is increased especially in the bladder urothelium after prostatic inflammation. We also confirmed that bladder overactivity and NGF upregulation in the bladder mucosa after prostatic inflammation are nerve-mediated and dependent on activation of the pelvic nerve, which contains bladder and prostate-innervating afferents. Taken together, our results suggest that prostatic inflammation induces bladder overactivity in association with NGF upregulation in the bladder as well as changes in ion channel expression and excitability of bladder afferent neurons due to afferent cross-sensitization from the prostate to bladder, possibly through activation of dichotomized afferent pathways that innervate both organs. The upregulation of TRPV1, TRPA1 and P2X2 channels, which are known to respond to noxious stimuli (Sun *et al.* 2010; Lee *et al.* 2016b), in combination with downregulation of the

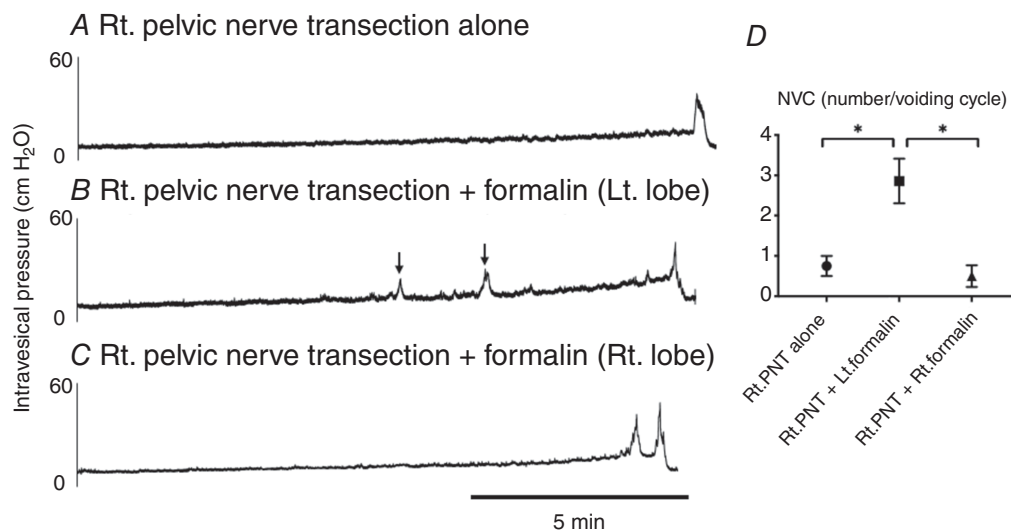


Figure 4. Single cystometry in rats with unilateral pelvic nerve transection

Representative traces of cystometry under an awake condition in rats with transection of the right pelvic nerve, which received no additional treatment (A), formalin injection into the contralateral side (left) of the ventral prostate lobe (B) or formalin injection into the ipsilateral side (right) of the ventral prostate lobe (C). D, the comparison of the number of non-voiding contraction (NVC) per voiding cycle shows that NVC are more frequent ($P < 0.05$) in pelvic nerve-transected rats with formalin injection into the left prostate lobe (Rt. PNT + Lt. formalin) compared to rats with Rt. PNT alone or PNT rats with the right lobe formalin injection (Rt. PNT + Rt. formalin) ($n = 7$ – 8 rats per group).

Kv1.4 potassium channel subunit, which can form slow K_A channels and suppress neuronal excitability (Hayashi *et al.* 2009; Takahashi *et al.* 2013), could lead to hyperexcitability of bladder afferent pathways, thereby inducing increased urinary frequency via activation of C-fibre afferent pathways after prostatic inflammation.

Based on these results of this study, the following mechanisms could be involved in bladder afferent activation after prostatic inflammation. When dichotomized afferents are irritated by intra-prostatic inflammation, it is possible that afferent nerves in the bladder are also be activated via action potentials propagating antidromically into the bladder through dichotomized afferents innervating both the bladder and prostate. Neurotransmitters released from afferent nerve terminals distributed in or near the urothelium could induce NGF expression, which would then stimulate and sensitize bladder afferent pathways (Ochodnický *et al.* 2012). Previous studies showed that NGF expression is significantly increased in the bladder urothelium without neutrophil infiltration following colitis (Kawamorita *et al.*

2016). Taken together, these sequential events including urothelial NGF upregulation through activation of dichotomized afferents innervating the prostate and the bladder may be involved in the mechanism by which prostatic inflammation contributes to storage LUTS in men with symptomatic BPH. In addition, other mechanisms such as spinal convergence of afferent nerves from different pelvic organs, increased urothelial permeability, mast cell activation in the bladder and/or neurogenic inflammation due to neuropeptide release from afferent nerve terminals have also been proposed in another model of pelvic organ cross-sensitization induced by experimental colitis (Grundy & Brierley, 2018), although further studies are needed to investigate whether these mechanisms similarly contribute to bladder overactivity induced by prostate-to-bladder cross-sensitization. In addition, the rat model of prostatic inflammation used in this study is not the direct model of BPH; however, we have shown that this rat model exhibits the upregulation of androgen receptor-responsive genes and TGF- β -related genes in the prostate (Funahashi

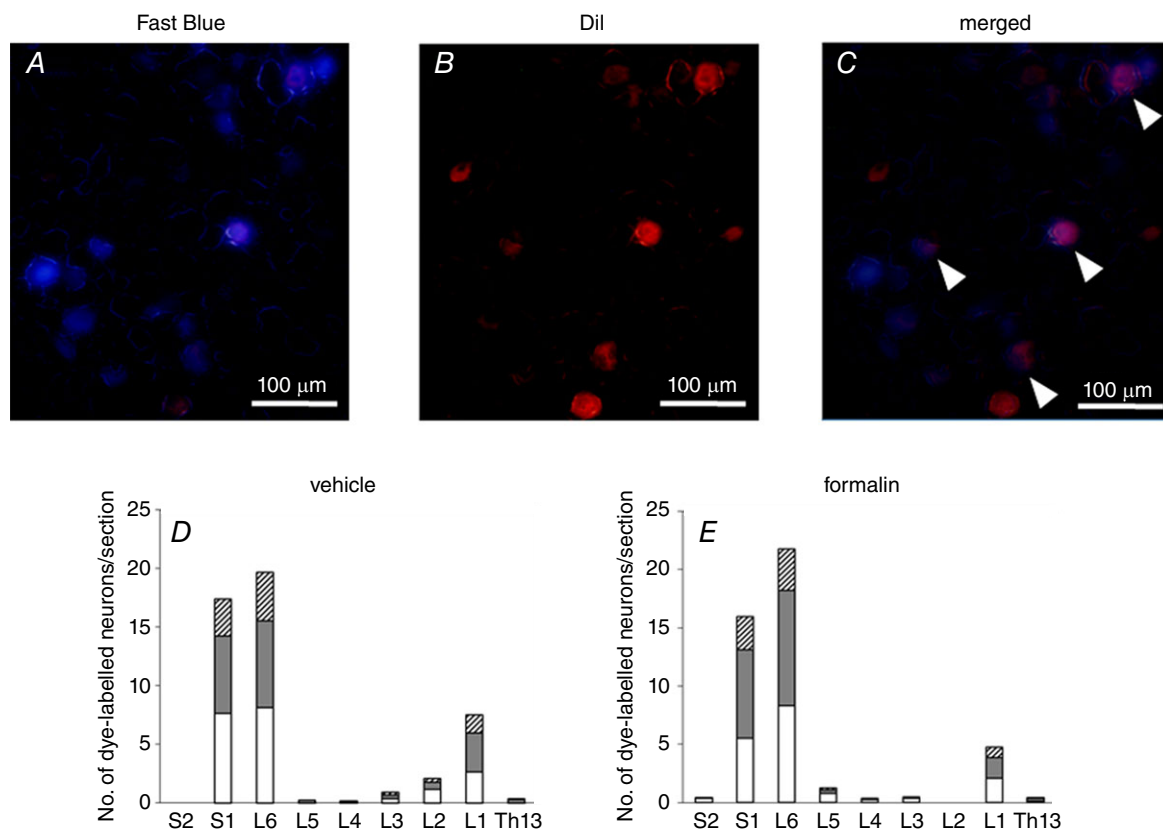


Figure 5. Fluorescent microscopic images of DRG sections

Representative fluorescent microscopic images of DRG neuron labelled with Fast Blue (A) and Dil (B) injected into the bladder wall and the ventral lobes of prostate, respectively. C, a merged image of A and B showed that some neurons were labelled with both dyes, as indicated by arrowheads. Scale bars; 100 μ m. The number of neurons dye-labelled with Fast Blue (white column), Dil (grey column) and both (hatched column) in sections of Th13 to S2 DRG from vehicle-injected (D) and formalin-injected rats (E) was quantified (6 DRG from 3 rats per groups). Columns represent the mean number of dye-labelled neurons per section.

Table 3. Action potential characteristics of capsaicin-sensitive DRG neurons

	Double-labelled afferent		Bladder afferent	
	Vehicle	Formalin	Vehicle	Formalin
Total no. of neurons/rats	8/5	7/5	8/5	10/5
Diameter (μm)	28.4 \pm 0.8	30.4 \pm 1.0	27.7 \pm 1.1	28.9 \pm 0.6
Input capacitance (pF)	27.0 \pm 1.5	37.5 \pm 3.2*	30.8 \pm 2.6	33.3 \pm 2.4
Membrane potential (mV)				
Resting	-50.3 \pm 1.2	-47.2 \pm 1.4	-50.8 \pm 0.9	-48.6 \pm 0.8
Spike threshold	-19.5 \pm 1.1	-28.3 \pm 1.4**	-21.6 \pm 2.4	-28.7 \pm 1.4*
Peak	36.3 \pm 2.2	46.3 \pm 2.6*	38.2 \pm 3.7	39.4 \pm 2.6
Spike duration (ms)	6.4 \pm 0.9	3.6 \pm 0.4*	5.6 \pm 0.7	4.4 \pm 0.4
No. of action potentials during 800 ms depolarization	1.2 \pm 0.1	5.1 \pm 0.7**	1.5 \pm 0.3	3.5 \pm 0.4**

* $P < 0.05$; ** $P < 0.01$ between vehicle and formalin groups.

et al. 2014), which is similarly seen in human BPH tissues (O'Malley *et al.* 2009), and that increased IL-18 expression induced by inflammasome activation is similarly found in the formalin-induced rat prostatic inflammation model (Kashyap *et al.* 2015) and in human

BPH specimens with inflammatory cell infiltration (Tyagi *et al.* 2017). Thus, the model of non-bacterial prostatic inflammation used in this study seems useful for investigating inflammation-related events that occur in human BPH with tissue inflammation.

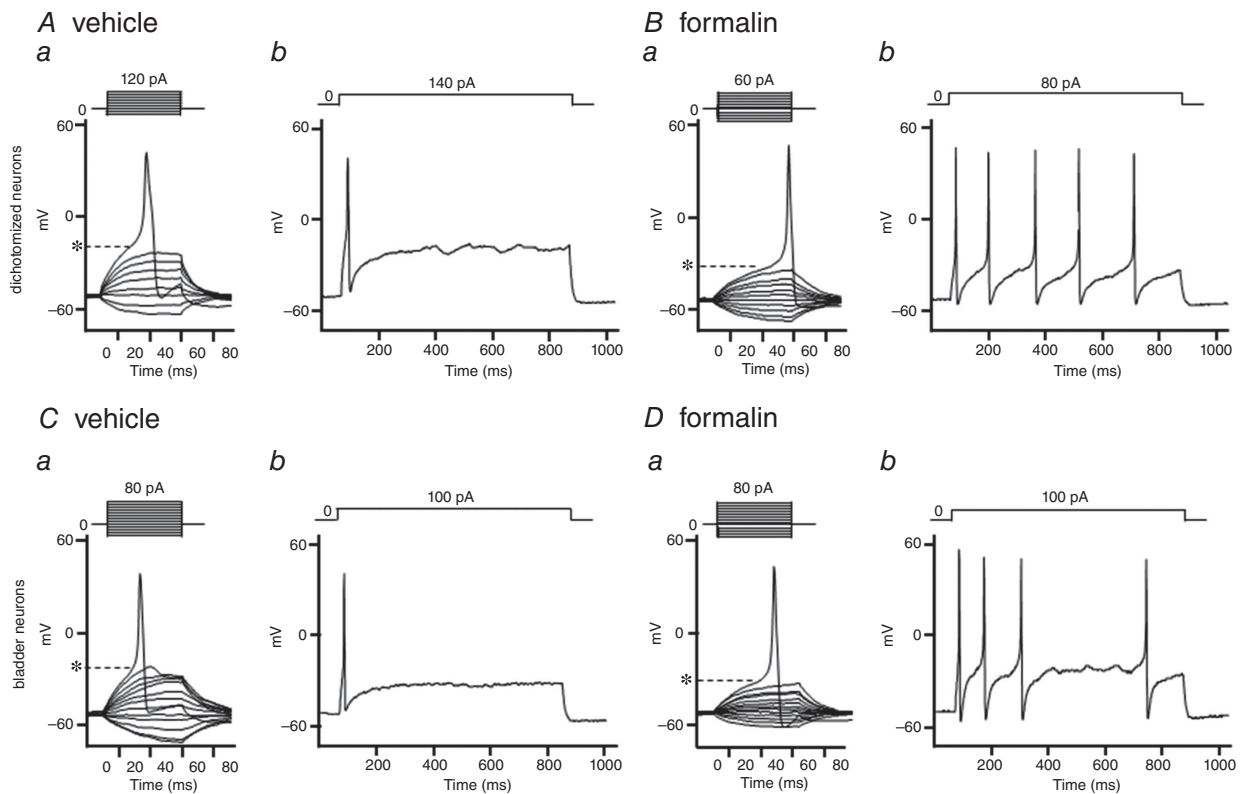


Figure 6. Action potential characteristics of capsaicin-sensitive double-labelled and Fast Blue-labelled afferent neurons

Representative recordings of action potentials in double-labelled, dichotomized afferent neurons from vehicle-injected (A) and formalin-injected rats (B), and Fast Blue-labelled bladder afferent neurons from vehicle-injected (C) and formalin-injected rats (D). The thresholds for eliciting action potentials (panels a of A–D) in formalin-injected rats was lower than those in vehicle-injected control rats (Aa vs. Ba or Ca vs. Da). The number of action potentials during 800 ms membrane depolarization (panels b of A–D) in formalin-injected rats was greater than that in control rats (Ab vs. Bb or Cb vs. Db). *Firing thresholds of action potentials.

Afferent neurons express various types of receptors and ion channels, including TRP channels, purinergic, muscarinic, endothelin, neurotrophic factor and estrogen receptors. TRPV1 and TRPA1 receptors overlap considerably in C-fibre afferent pathways in rats (La *et al.* 2011), and their functional interaction has been reported (Salas *et al.* 2009; Staruschenko *et al.* 2010). Also, approximately 90% of the bladder afferent neurons are excited by ATP, which induces depolarization and firing mainly through activation of P2X2/3 receptors rather than P2X3 receptors (Zhong *et al.* 2003; Dang *et al.* 2005). Thus, the increased expression of TRPV1, TRPA1 and P2X2 receptors found in this study in both dichotomized and bladder afferent neurons in

rats with prostatic inflammation, which could enhance responses of bladder afferents to noxious stimuli such as ATP, could contribute to C-fibre bladder afferent hyperexcitability and bladder overactivity following prostatic inflammation. Only a few previous studies have reported changes in the expression of these receptors in visceral afferents, probably because only a limited number of neurons in L6-S1 DRG innervate the pelvic viscera (Yoshimura *et al.* 1998; Christianson *et al.* 2007; Chen *et al.* 2010). Thus, the LCM method in combination with axonal tracing was essential in our experiments for detecting the pathology-induced plasticity in prostate and bladder afferent neurons. However, since protein levels were not analysed in this study because of the low amount

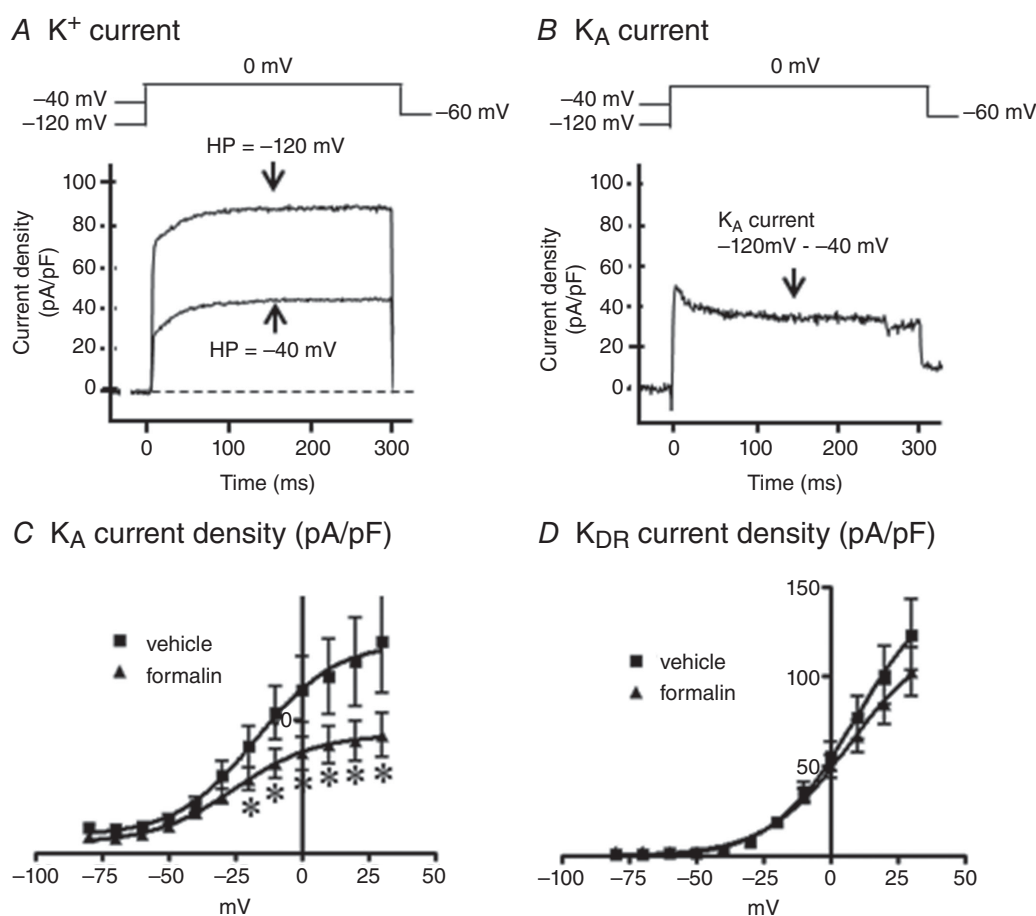


Figure 7. Changes of K⁺ currents in capsaicin-sensitive bladder afferent neurons

A, representative recordings in a capsaicin-sensitive bladder afferent neuron from a control rat showing superimposed outward K⁺ currents evoked by depolarizing voltage pulses to 0 mV from holding potentials (HPs) of -120 and -40 mV and sustained delayed rectifier-type K⁺ (sustained K_{DR}) currents evoked by depolarization from -40 mV HP. **B**, representative recordings in a capsaicin-sensitive bladder afferent neuron from a control rat showing slow decaying A-type K⁺ (slow K_A) currents obtained by subtracting K⁺ currents evoked by depolarization from HP of -40 to 0 mV from the K⁺ currents evoked by depolarization from HP of -120 mV to 0 mV. **C**, *I-V* relationships of slow K_A currents showing that the density of K_A currents in capsaicin-sensitive bladder afferent neurons from formalin-injected rats (*n* = 9 cells from 9 rats) was significantly reduced compared to that from vehicle-injected rats (*n* = 9 cells from 9 rats). **D**, *I-V* relationships of sustained K_{DR} currents showing that the density of K_{DR} currents was not significantly different between two groups (*n* = 10 cells from 8 rats each). **P* < 0.05 compared to vehicle-injected rats (Student's unpaired *t* test).

of proteins in neurons collected by LCM, further analyses using immunohistochemistry with validation of antibody specificity will be necessary.

The whole-cell patch-clamp recordings described herein demonstrated that prostatic inflammation induced hyperexcitability of bladder and dichotomized afferent neurons (i.e. prostate and bladder double-innervating). Under the current-clamp recording conditions, we observed an increase of cell input capacitance, which corresponds to cell surface area, and shortening of spike duration in the double-labelled afferent neurons, but not the bladder afferent neurons, of the formalin-injected rats. Thus, we speculate that the direct sensitization of double-labelled neurons innervating the inflamed prostate leads to more profound changes in these parameters compared to bladder afferent neurons, in which sensitization was induced indirectly after prostatic inflammation. Furthermore, it is likely that changes of excitability in bladder afferent neurons are mediated at least in part by reduced expression of the Kv1.4 voltage-gated potassium channel subunit and decreased slow K_A current density. Among the many types of potassium channels, Kv1.4 is a major molecular subunit of the A-type potassium channel, which suppresses neuronal depolarization (Zhong *et al.* 2003). We previously

reported that a reduction in Kv1.4 subunit expression detected by immunohistochemistry is associated with reduced A-type potassium channel activity and hyperexcitability of capsaicin-sensitive C-fibre bladder afferent neurons in rats with hydrochloric acid-induced cystitis (Hayashi *et al.* 2009) and spinal cord injury (Takahashi *et al.* 2013). Furthermore, NGF application induces hyperexcitability of bladder afferent neurons by decreasing A-type potassium channel activity in normal rats (Yoshimura *et al.* 2006). Thus, this study suggests that the reduction in Kv1.4 expression, which is possibly induced by NGF upregulation in the bladder, contributes directly to capsaicin-sensitive C-fibre bladder afferent hyperexcitability induced by prostate-to-bladder afferent cross-sensitization following prostatic inflammation, although further studies are needed to confirm that NGF upregulation is a mediator in this process.

In conclusion, chemically induced inflammation localized in the prostate induces bladder overactivity and upregulation of NGF expression in the bladder urothelium. Bladder afferent function was enhanced as indicated by TRPV1, TRPA1 and P2X2 upregulation, Kv1.4 downregulation, and cell hyperexcitability. Since there is a clinical association between prostatic inflammation and BPH-induced LUTS, the

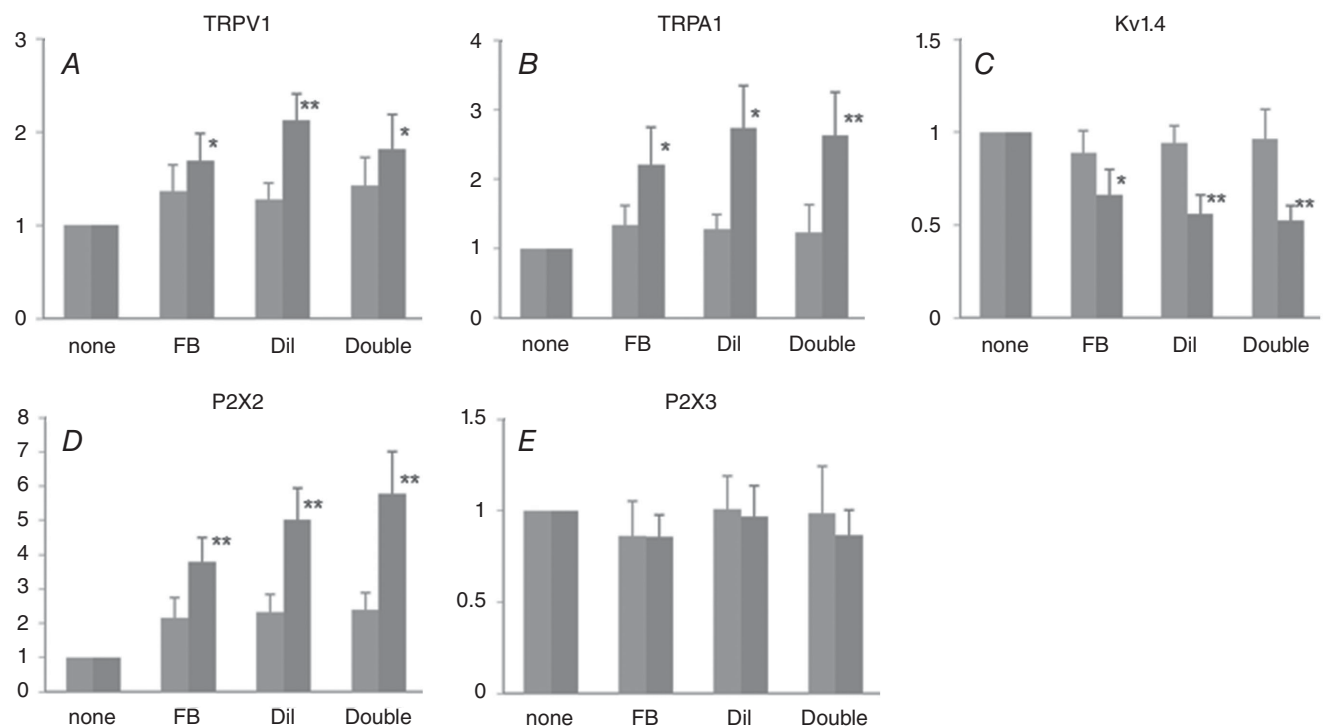


Figure 8. Relative mRNA levels in the afferent neurons

Fast Blue (FB)-, Dil-, and double-labelled neurons in DRG sections were dissected by LCM, and mRNA levels of TRPV1 (A), TRPA1 (B), Kv1.4 (C), P2X2 (D) and P2X3 (E) were measured by qRT-PCR and expressed relative to the levels expressed in non-labelled neurons. Light grey columns, vehicle-treated rats ($n = 10$). Dark grey columns, formalin-treated rats ($n = 11$). Columns with bars represent means \pm SEM. * $P < 0.05$, ** $P < 0.01$ compared to non-labelled neurons.

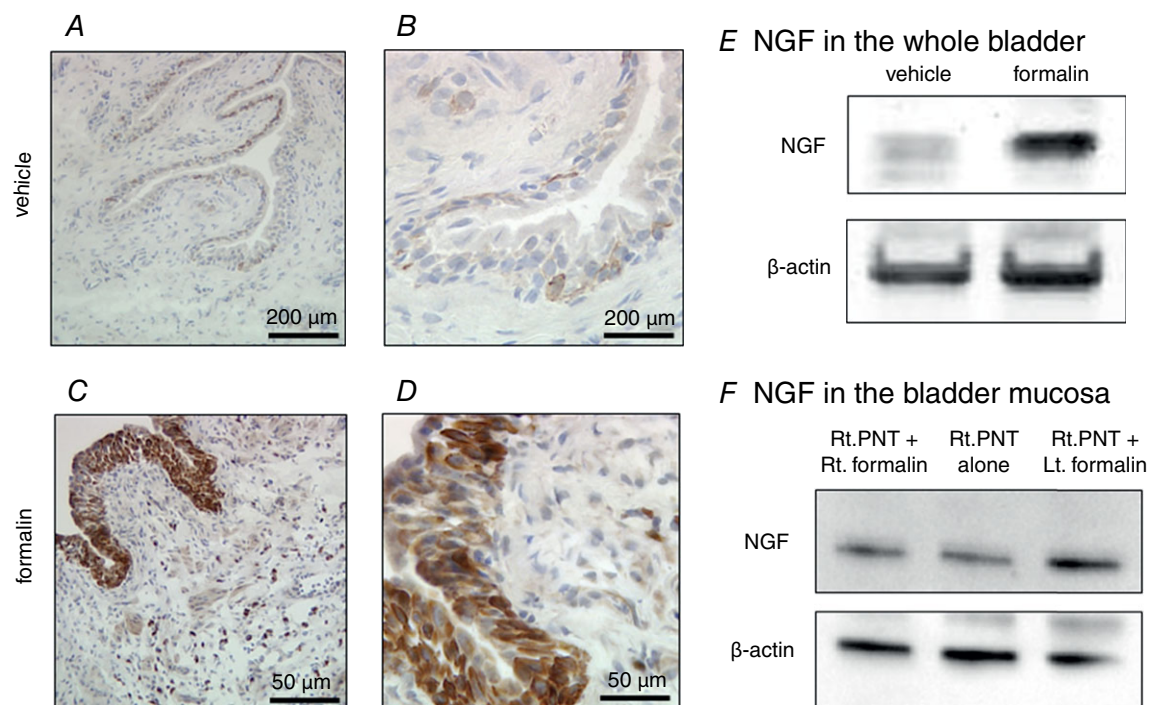


Figure 9. NGF expression in the bladder

NGF expression was markedly enhanced in formalin-injected rats, especially in the urothelium (C, D), compared to the vehicle-injected controls (A, B). Scale bars; 200 μm (A, C) and 50 μm (B, D). Western blotting in bladder tissue extracts showed upregulation of NGF expression in the formalin-injected compared to vehicle-injected rats (E). F, in rats with the right pelvic nerve transection (PNT), formalin injection into the left ventral lobe of prostate induced NGF upregulation in the bladder mucosa (Rt. PNT + Lt. formalin) compared to rats with PNT alone (Rt. PNT alone); however, increased NGF expression was not seen when formalin was injected into the right ventral lobe of prostate (Rt. PNT + Rt. formalin).

prostate-to-bladder cross-sensitization through primary afferent pathways in the pelvic nerve, which contains dichotomized afferents, is a potentially important mechanism contributing to bladder overactivity and afferent hyperexcitability after prostatic inflammation, which can cause storage LUTS in symptomatic BPH patients.

References

- Aydin M, Wang HZ, Zhang X, Chua R, Downing K, Melman A & DiSanto ME (2012). Large-conductance calcium-activated potassium channel activity, as determined by whole-cell patch clamp recording, is decreased in urinary bladder smooth muscle cells from male rats with partial urethral obstruction. *BJU Int* **110**, E402–E408.
- Beppu M, Araki I, Yoshiyama M, Du S, Kobayashi H, Zakoji H & Takeda M (2011). Bladder outlet obstruction induced expression of prostaglandin E2 receptor subtype EP4 in the rat bladder: a possible counteractive mechanism against detrusor overactivity. *J Urol* **186**, 2463–2469.
- Brumovsky PR & Gebhart GF (2010). Visceral organ cross-sensitization – an integrated perspective. *Autonom Neurosci* **153**, 106–115.
- Chen Y, Wu X, Liu J, Tang W, Zhao T & Zhang J (2010). Distribution of convergent afferents innervating bladder and prostate at dorsal root ganglia in rats. *Urology* **76**, 764.e1–6.
- Christianson JA, Liang R, Ustinova EE, Davis BM, Fraser MO & Pezzone MA (2007). Convergence of bladder and colon sensory innervation occurs at the primary afferent level. *Pain* **128**, 235–243.
- Chung JH, Yu JH, Sung LH, Noh CH & Chung JY (2012). Effect of prostatitis on lower urinary tract symptoms: retrospective analysis of prostate biopsy tissue. *Korean J Urol* **53**, 109–113.
- Dang K, Bielefeldt K & Gebhart GF (2005). Differential responses of bladder lumbosacral and thoracolumbar dorsal root ganglion neurons to purinergic agonists, protons, and capsaicin. *J Neurosci* **25**, 3973–3984.
- de Groat WC, Griffiths D & Yoshimura N (2015). Neural control of the lower urinary tract. *Compr Physiol* **5**, 327–396.
- Fibbi B, Penna G, Morelli A, Adorini L & Maggi M (2010). Chronic inflammation in the pathogenesis of benign prostatic hyperplasia. *Int J Androl* **33**, 475–488.
- Funahashi Y, Hattori R, Matsukawa Y, Komatsu T, Sassa N & Gotoh M (2011). Clinical efficacy of a loading dose of naftopidil for patients with benign prostate hyperplasia. *World J Urol* **29**, 225–231.
- Funahashi Y, O'Malley KJ, Kawamorita N, Tyagi P, DeFranco DB, Takahashi R, Gotoh M, Wang Z & Yoshimura N (2014). Upregulation of androgen-responsive genes and

- transforming growth factor-beta1 cascade genes in a rat model of non-bacterial prostatic inflammation. *Prostate* **74**, 337–345.
- Grundy L & Brierley SM (2018). Cross-organ sensitization between the colon and bladder: to pee or not to pee? *Am J Physiol Gastrointest Liver Physiol* **314**, G301–G308.
- Hayashi Y, Takimoto K, Chancellor MB, Erickson KA, Erickson VL, Kirimoto T, Nakano K, de Groat WC & Yoshimura N (2009). Bladder hyperactivity and increased excitability of bladder afferent neurons associated with reduced expression of Kv1.4 alpha-subunit in rats with cystitis. *Am J Physiol Regul Integr Comp Physiol* **296**, R1661–R1670.
- Kashyap M, Pore S, Wang Z, Gingrich J, Yoshimura N & Tyagi P (2015). Inflammasomes are important mediators of prostatic inflammation associated with BPH. *J Inflamm (Lond)* **12**, 37.
- Kawamori N, Yoshikawa S, Kashyap M, Tyagi P, Arai Y, Chancellor MB & Yoshimura N (2016). Liposome based intravesical therapy targeting nerve growth factor ameliorates bladder hypersensitivity in rats with experimental colitis. *J Urol* **195**, 1920–1926.
- Kim SO, Oh BS, Chang IY, Song SH, Ahn K, Hwang EC, Oh KJ, Kwon D & Park K (2011). Distribution of interstitial cells of Cajal and expression of nitric oxide synthase after experimental bladder outlet obstruction in a rat model of bladder overactivity. *NeuroUrol Urodyn* **30**, 1639–1645.
- La JH, Schwartz ES & Gebhart GF (2011). Differences in the expression of transient receptor potential channel V1, transient receptor potential channel A1 and mechanosensitive two pore-domain K⁺ channels between the lumbar splanchnic and pelvic nerve innervations of mouse urinary bladder and colon. *Neuroscience* **186**, 179–187.
- Lee S, Yang G & Bushman W (2015). Prostatic inflammation induces urinary frequency in adult mice. *PLoS One* **10**, e0116827.
- Lee S, Yang G, Xiang W & Bushman W (2016a). Retrograde double-labeling demonstrates convergent afferent innervation of the prostate and bladder. *Prostate* **76**, 767–775.
- Lee WC, Wu CC, Chuang YC, Tain YL & Chiang PH (2016b). Ba-Wei-Die-Huang-Wan (Hachimi-jio-gan) can ameliorate cyclophosphamide-induced ongoing bladder overactivity and acidic adenosine triphosphate solution-induced hyperactivity on rats prestimulated bladder. *J Ethnopharmacol* **184**, 1–9.
- Liao CH, Chung SD & Kuo HC (2011). Serum C-reactive protein levels are associated with residual urgency symptoms in patients with benign prostatic hyperplasia after medical treatment. *Urology* **78**, 1373–1378.
- Lin WY, Guven A, Juan YS, Neuman P, Whitbeck C, Chichester P, Kogan B, Levin RM & Mannikarottu A (2008). Free radical damage as a biomarker of bladder dysfunction after partial outlet obstruction and reversal. *BJU Int* **101**, 621–626.
- Malykhina AP (2007). Neural mechanisms of pelvic organ cross-sensitization. *Neuroscience* **149**, 660–672.
- Mizoguchi S, Mori K, Wang Z, Liu T, Funahashi Y, Sato F, DeFranco DB, Yoshimura N & Mimata H (2017). Effects of estrogen receptor beta stimulation in a rat model of non-bacterial prostatic inflammation. *Prostate* **77**, 803–811.
- Nickel JC, Roehrborn CG, O’Leary MP, Bostwick DG, Somerville MC & Rittmaster RS (2008). The relationship between prostate inflammation and lower urinary tract symptoms: examination of baseline data from the REDUCE trial. *Eur Urol* **54**, 1379–1384.
- O’Malley KJ, Dhir R, Nelson JB, Bost J, Lin Y & Wang Z (2009). The expression of androgen-responsive genes is up-regulated in the epithelia of benign prostatic hyperplasia. *Prostate* **69**, 1716–1723.
- Ochodnický P, Cruz CD, Yoshimura N & Cruz F (2012). Neurotrophins as regulators of urinary bladder function. *Nat Rev Urol* **9**, 628–637.
- Robert G, Descazeaud A, Nicolaiew N, Terry S, Sirab N, Vacherot F, Maille P, Allory Y & de la Taille A (2009). Inflammation in benign prostatic hyperplasia: a 282 patients’ immunohistochemical analysis. *Prostate* **69**, 1774–1780.
- Salas MM, Hargreaves KM & Akopian AN (2009). TRPA1-mediated responses in trigeminal sensory neurons: interaction between TRPA1 and TRPV1. *Eur J Neurosci* **29**, 1568–1578.
- Schwartz ES, La JH, Young EE, Feng B, Joyce S & Gebhart GF (2016). Chronic prostatitis induces bladder hypersensitivity and sensitizes bladder afferents in the mouse. *J Urol* **196**, 892–901.
- Staruschenko A, Jeske NA & Akopian AN (2010). Contribution of TRPV1-TRPA1 interaction to the single channel properties of the TRPA1 channel. *J Biol Chem* **285**, 15167–15177.
- Sun B, Li Q, Dong L & Rong W (2010). Ion channel and receptor mechanisms of bladder afferent nerve sensitivity. *Auton Neurosci* **153**, 26–32.
- Takahashi R, Yoshizawa T, Yunoki T, Tyagi P, Naito S, de Groat WC & Yoshimura N (2013). Hyperexcitability of bladder afferent neurons associated with reduction of Kv1.4 alpha-subunit in rats with spinal cord injury. *J Urol* **190**, 2296–2304.
- Tyagi P, Kashyap M, Gingrich J, Wang Z & Yoshimura N (2017). Inflammasome activation leads to IL-18 expression in prostatic inflammation associated with BPH. *J Urol* **197**, e211–212.
- Yoshimura N, Bennett NE, Hayashi Y, Ogawa T, Nishizawa O, Chancellor MB, de Groat WC & Seki S (2006). Bladder overactivity and hyperexcitability of bladder afferent neurons after intrathecal delivery of nerve growth factor in rats. *J Neurosci* **26**, 10847–10855.
- Yoshimura N & de Groat WC (1997). Plasticity of Na⁺ channels in afferent neurones innervating rat urinary bladder following spinal cord injury. *J Physiol* **503**, 269–276.
- Yoshimura N & de Groat WC (1999). Increased excitability of afferent neurons innervating rat urinary bladder after chronic bladder inflammation. *J Neurosci* **19**, 4644–4653.
- Yoshimura N, Erdman SL, Snider MW & de Groat WC (1998). Effects of spinal cord injury on neurofilament immunoreactivity and capsaicin sensitivity in rat dorsal root ganglion neurons innervating the urinary bladder. *Neuroscience* **83**, 633–643.
- Zhong Y, Banning AS, Cockayne DA, Ford AP, Burnstock G & McMahon SB (2003). Bladder and cutaneous sensory neurons of the rat express different functional P2X receptors. *Neuroscience* **120**, 667–675.

Additional information**Competing interests**

The authors have declared that no conflict of interest exists.

Author contributions

Y.F., R.T., Z.W., D.B.D. and N.Y. created the research design. Y.F., R.T., T.S., E.T. and S.M. performed experiments and analysed data. Y.F., R.T., T.S., P.T. and N.Y. interpreted the results of experiments. Y.F., R.T., W.C.dG. and N.Y. drafted the manuscript. Y.F.,

R.T., T.S., E.T., S.M., J.N., Z.W., D.B.D., W.C.dG., P.T. and N.Y. approved the final version of manuscript. All authors agree to be accountable for all aspects of the work. All persons designated as authors qualify for authorship, and all those who qualify for authorship are listed.

Funding

This work was supported by a grant from the National Institutes of Health National Institute of Diabetes and Digestive and Kidney (U54 DK112079).